

RESEARCH ARTICLE

Two chiral types of randomly rotated ommatidia are distributed across the retina of the flathead oak borer *Coraebus undatus* (Coleoptera: Buprestidae)

Andrej Meglič¹, Marko Ilić², Carmen Quero³, Kentaro Arikawa² and Gregor Belušič^{4,*}

ABSTRACT

Jewel beetles are colorful insects, which use vision to recognize their conspecifics and can be lured with colored traps. We investigated the retina and coloration of one member of this family, the flathead oak borer *Coraebus undatus* using microscopy, spectrometry, polarimetry, electroretinography and intracellular recordings of photoreceptor cell responses. The compound eyes are built of a highly unusual mosaic of mirror-symmetric or chiral ommatidia that are randomly rotated along the body axes. Each ommatidium has eight photoreceptors, two of them having rhabdomeres in tiers. The eyes contain six spectral classes of photoreceptors, peaking in the UV, blue, green and red. Most photoreceptors have moderate polarization sensitivity with randomly distributed angular maxima. The beetles have the necessary retinal substrate for complex color vision, required to recognize conspecifics and suitable for a targeted design of color traps. However, the jewel beetle array of freely rotated ommatidia is very different from the ordered mosaic in insects that have object-directed polarization vision. We propose that ommatidial rotation enables the cancelling out of polarization signals, thus allowing stable color vision, similar to the rhabdomeric twist in the eyes of flies and honeybees.

KEY WORDS: Jewel beetle, Compound eye, Spectral sensitivity, Polarization sensitivity, Retinal mosaic

INTRODUCTION

Jewel beetles (Coleoptera: Buprestidae) get their name from their iridescent cuticles resembling jewelry (Fig. 1). Their exoskeleton consists of alternating multilayers of chitin with different refractive indices, which create a bright iridescent display (Hariyama et al., 2005; Schenk et al., 2013; Stavenga et al., 2011; Vigneron et al., 2006). In jewel beetles, visual cues such as color, texture and body shape, together with short- and long-range olfactory cues are essential to locate hosts and mates (Domingue and Baker, 2012; Poland et al., 2019). Many species are agricultural pests that can be successfully lured by decoys in the form of dead or artificial specimens, by colored plastic funnels or sheets coated with glue.

Species from *Agrilus* and *Coraebus* genera are attracted by green- or purple-colored traps, respectively (Francese et al., 2010; Fürstenau et al., 2015; Imrei et al., 2020). More importantly, in some beetles, the cuticular reflections are linearly polarized, suggesting that the beetles could use object-directed (or ‘non-celestial’) polarization vision in intraspecific communication (Stavenga et al., 2011). If this is the case, then their retina should be equipped with sets of polarization-sensitive photoreceptor cells, occurring in opponent pairs with different angular maxima of polarization sensitivity.


Polarization vision for detecting celestial polarization is in many insects mediated by photoreceptors in the dorsal rim area of their compound eyes (Labhart, 2016). Object-directed polarization vision, mediated by retinal photoreceptors apart from those in the dorsal rim, has been demonstrated in, for example, horseflies and butterflies (Bandai et al., 1992; Blake et al., 2019a,b; Kinoshita et al., 2011; Meglič et al., 2019). The photoreceptors of these insects, which are specialized for color or polarization vision, are packed within the ommatidia in a highly ordered pattern, so that homologous photoreceptor cells always occur under the same angles. For instance, the retina of horseflies is composed of two randomly distributed ommatidial types, where the pairs of polarization detectors in a single type have horizontal and vertical microvilli (Meglič et al., 2019). The retina of butterflies contains three stochastically distributed ommatidial types, where the microvilli of homologous receptors occur under identical – vertical, horizontal and diagonal – orientation (Wernet et al., 2015; Arikawa, 2017; Blake et al., 2019b). Even if insect photoreceptors are not optimized for polarization vision, their intrinsic polarization sensitivity can destabilize color or motion vision and lead to polarization-dependent artifacts (Kelber et al., 2001). To avoid this problem, insects have evolved photoreceptors with minimized polarization sensitivity, having microvilli rotated or twisted along the rhabdomere (Smola and Wunderer, 1981; Wehner and Bernard, 1993). Polarization sensitivity can also be minimized at the level of the interneurons, by pooling of signals from photoreceptors with phase-shifted polarization sensitivity maxima. This solution, for instance, minimizes polarization sensitivity of lamina monopolar cells (LMCs) in flies and butterflies (Hardie, 1985; Chen et al., 2020).

The beetle retinal mosaic remains little studied. Photoreceptor recordings in the seven-spot ladybird, *Coccinella septempunctata* (Coleoptera: Coccinellidae), suggest that the photoreceptors in the retinal mosaic have stereotyped microvillar directions (Lin, 1993). However, a single published study on the retinal anatomy of the buprestid *Curis caloptera* shows an ommatidial array where homologous photoreceptors appear to have randomly oriented microvilli (Gokan and Meyer-Rochow, 1984).

We were curious to find out what exactly in the purple traps attracted *Coraebus* beetles: the blue and/or the red, or the polarized

¹Eye Hospital, University Medical Centre, Grablovičeva 46, 1000 Ljubljana, Slovenia. ²Laboratory of Neuroethology, Sokendai – The Graduate University for Advanced Studies, Hayama 240-0193, Japan. ³Department of Biological Chemistry and Molecular Modelling, IQAC (CSIC), Jordi Girona 18-26, 08034 Barcelona, Spain. ⁴Department of Biology, Biotechnical Faculty, University of Ljubljana, Večna pot 111, 1000 Ljubljana, Slovenia.

*Author for correspondence (gregor.belusic@bf.uni-lj.si)

 A.M., 0000-0003-3837-8108; M.I., 0000-0001-9910-0359; C.Q., 0000-0003-3599-2778; K.A., 0000-0002-4365-0762; G.B., 0000-0003-3571-1948

reflections. If the beetles were indeed able to see the trap in all its complexity, they should be equipped with an extended set of spectral photoreceptors, probably peaking in the blue, green and red parts of the spectrum. Certain groups of beetles have been reported to be lacking the short wavelength-sensitive (SW) opsins that confer sensitivity to blue (Jackowska et al., 2007; Sharkey et al., 2017). Buprestid beetles, however, have supposedly overcome the evolutionary loss with duplications of UV and long wavelength-sensitive (LW) opsins, ending with up to five opsins in their genome (Lord et al., 2016). Thus, we expected to find a jewel beetle with a complex set of spectral receptors. If the oak borers utilize polarization vision for object detection, then their ommatidia should be equipped with ordered photoreceptors with high polarization sensitivity. We used the oak borer *Coraebus undatus* to investigate the jewel beetle retinal substrate for color and polarization vision. We analyzed the anatomy of the retina using light and electron microscopy, and we studied the spectral and polarization properties of the photoreceptors using extracellular as well as single-cell, intracellular recordings. To interpret the visual functions of the photoreceptors, we performed spectrophotometric and polarimetric measurements of beetle cuticle and the trap.

MATERIALS AND METHODS

Animals

Adult beetles, *Coraebus undatus* (Fabricius 1787), were collected in cork oak woods at Arbúcies (Catalonia, Spain) and shipped on ice to Ljubljana (Slovenia). After recordings, the beetles were preserved in ethanol and their sex was determined. The recordings were made in the total of 11 beetles (5 females, 6 males). Three beetles were used for anatomy. Cuticular coloration was measured in two specimens.

Anatomy

Isolated retinæ were pre-fixed for 3 h in 4% paraformaldehyde and 3.5% glutaraldehyde, post-fixed for 90 min in 0.1 mol l⁻¹ OsO₄ in 0.1 mol l⁻¹ Na cacodylate, pH 7.2, dehydrated in an ethanol series, and then embedded in Spurr's resin. Semi-thin sections (1 µm) for light microscopy and ultrathin sections were cut on an Ultracut S ultramicrotome (Leica, Nussloch, Germany) with a diamond knife (Diatome, Nidau, Switzerland). The semi-thin sections were stained with Azur II. The sections were observed with an Axiomager Z.1 (Zeiss, Oberkochen, Germany) light microscope and an H-7650 transmission electron microscope (Hitachi, Tokyo, Japan).

Semi-thin cross-sections of the proximal retina were used to determine ommatidial chirality in larger assemblages, containing up to ~150 ommatidia. In images, obtained with a 63× oil immersion objective and digitally elevated contrast, the crystalline cone extensions (CCE) could be resolved as quadruples of varicosities, bordering the somata of certain photoreceptor cells (circular insets in Fig. 4C). The largest soma was that of R8. Ommatidial chirality was determined as clockwise (CW) or counter-clockwise (CCW) according to the rotation direction of cell numbering R1–8 (Figs 3B–D, 4A; Gokan and Meyer-Rochow; 1984).

Electrophysiological recordings

The spectral and polarization sensitivities of photoreceptors were measured by performing intracellular recordings in dark-adapted animals, using a high impedance amplifier (SEC-10LX, NPI, Tamm, Germany) in bridge mode. The electrodes, pulled from borosilicate glass on a horizontal puller (P-2000, Sutter, Novato, CA, USA), filled with 3 mol l⁻¹ KCl, had a resistance in the range 100–150 MΩ. The reference electrode was a 50 µm diameter Ag/AgCl wire, inserted into the head capsule next to the eye. The

animals were positioned on a custom-made goniometer, carrying the immobilized insect and a piezo-driven micromanipulator (Sensapex, Oulu, Finland). The light stimuli were provided by a 'classical' photostimulator consisting of a 75 W xenon arc lamp (Cairn Research, Faversham, Kent, UK), a monochromator (B&M Optik, Limburg, Germany), a shutter, a computer-controlled neutral density wedge filter (Thorlabs, Dachau, Germany) and a UV-capable polarizer OUV2500 (Knight Optical, UK). We also used an LED synth, a light source based on LEDs and a diffraction grating (Belušič et al., 2016). Extracellular recordings yielding mass responses (electroretinogram, ERG) of the compound eyes were performed with blunt borosilicate electrodes, filled with insect

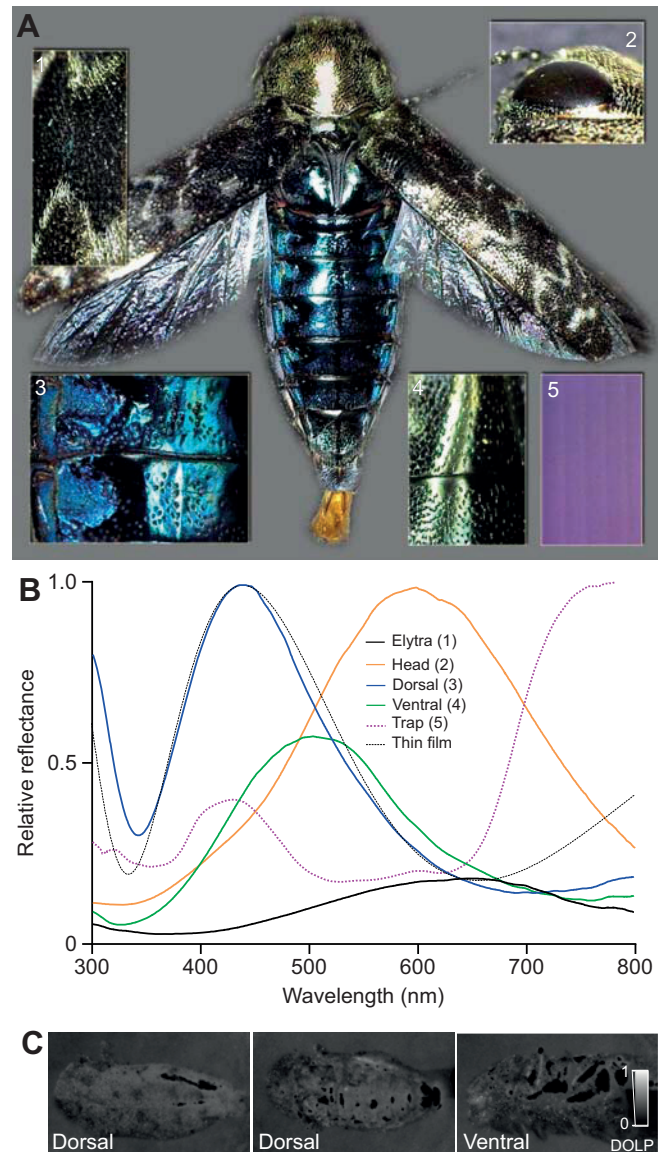


Fig. 1. External appearance and coloration of *Coraebus undatus* and the trap. (A) Macro photo of a male beetle, specimen length 15 mm. Insets: (1) elytra, (2) head, (3) dorsal abdomen, (4) ventral abdomen, (5) plastic trap. (B) Reflectance spectra of body parts and objects in A; spectra (1–4) were normalized to the peak reflectance of the dorsal abdominal cuticle (3). Black dotted line is the reflectance spectrum calculated for a 212 nm chitinous thin film. (C) Polarimetric images showing the degree of linear polarization (DOLP) of a beetle. Dorsal aspect, with (left) or without (middle) elytrae; ventral aspect (right). DOLP is coded with gray scale; black patches are overexposed; monochrome polarimetric image of the blue channel (450±20 nm).

Ringer solution (0.67% NaCl, 0.015% KCl, 0.012% CaCl₂, 0.015% NaHCO₃, pH 7.2). For extracellular recordings (ERG with selective adaptation), the eyes were selectively adapted using isoquantal light from the monochromator and the sensitivity was scanned with the LED synth.

The response amplitudes were transformed to sensitivities using the intensity–response function and reverse Hill transformation; spectral and polarization sensitivities were calculated as described previously (Meglič et al., 2019).

Spectrophotometry and polarimetry

Reflectance spectra of the beetle's cuticle and the purple plastic trap that was used in Fürstenau et al. (2015) were measured with a Flame spectrophotometer (Ocean Optics, Dunedin, FL, USA). The light source was a 150 W stabilized xenon arc lamp (66475-150XV-R22, Newport Corp., Irvine, CA, USA), and the reference was a MgO block. Degree of polarization of the cuticle was measured with a Phoenix PHX050S-P polarimetric camera (Lucid Vision Labs, Ilsfeld, Germany), fitted with a quartz objective (Ricoh, Tokyo, Japan) and bandpass filters with bandwidth 40 nm, center wavelength 360 nm (with IR blocking coating; Chroma Technology Corp, Bellows Falls, VT, USA), 450, 525, 600 nm (Techspec, Edmund Optics, York, UK) and analyzed with ArenaView software (Lucid Vision Labs).

Thin film reflectance calculation

To calculate the reflectance spectrum, the cuticle was modeled as a three-layered structure [air, refractive index (RI)=1; cuticle, RI=1.5; water, RI=1.3], using an online tool (<https://www.filmetrics.com/reflectance-calculator>).

RESULTS

Coloration

The flathead oak borer, when not flying, is an inconspicuous, mid-sized beetle (length 15 mm; Fig. 1A). Most of its body is covered

with black elytrae, decorated with thin white zig-zag lines, formed by white hairs. When the elytrae are extended, the shiny blue abdominal cuticle is displayed. The abdomen is green ventrally, and the cuticle on the head appears golden. The reflectance spectra of the colorful body parts have peak wavelengths at 440 nm (dorsal abdomen), 510 nm (ventral abdomen) and 600 nm (head) (Fig. 1B). The purple plastic trap has reflectance bands peaking at 430 and 750 nm; the reflectance band in the blue wavelength range resembles and possibly mimics the reflectance band of the beetle's blue abdominal cuticle. The spectrum of the blue cuticle is consistent with that of a chitinous thin film with 212 nm thickness (Fig. 1B). The cuticular reflectance is weakly linearly polarized, with a degree of linear polarization (DOLP)<0.25 (Fig. 1C).

Anatomy of the compound eyes

The compound eyes (radii ~1.5×0.8 mm) are composed of ~2800 ommatidia each (Fig. 2). The corneal facet lenses have a diameter of ~24 μm and the dioptrical apparatus is ~150 μm thick. The distal and proximal retina are densely pigmented with screening pigment granules in the pigment and photoreceptor cells (Fig. 3A). Each ommatidium contains 8 photoreceptor cells, forming a fused rhabdom (Fig. 3B–D; note that these panels present sections of three distinct ommatidia, each differently rotated with respect to the eye axes). Two cells, R7 and R8, have rhabdomeres in a restricted stretch of the retina, i.e. the R7 rhabdomere exists only in the distal tier and the R8 rhabdomere is only in the proximal tier. Thus, the distal rhabdom is composed of seven rhabdomeres, the middle rhabdom is composed of eight rhabdomeres, and the proximal rhabdom is composed mostly of the R8 rhabdomere (Fig. 4A; Fig. S1).

Each ommatidium contains four large crystalline cone extensions (CCEs) stretching throughout the entire length of the retina. The CCEs occur at the borders between photoreceptor cells in a conspicuous pattern: a single photoreceptor cell (here termed R2, following Gokan and Meyer-Rochow, 1984) is bordered by two

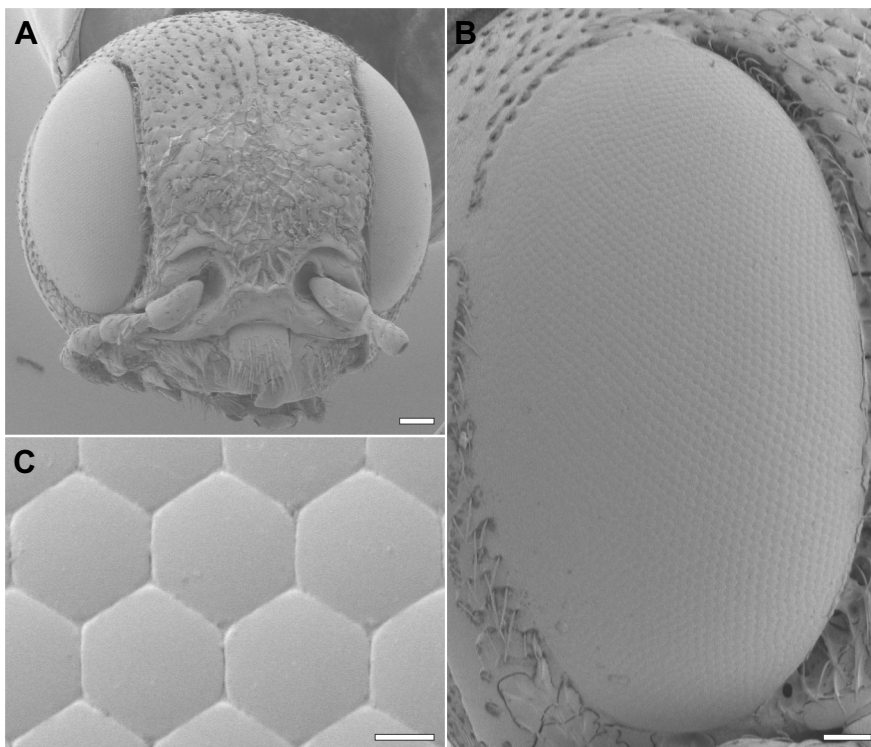


Fig. 2. External anatomy of the visual system.

Scanning electron micrographs of the (A) head, (B) right eye and (C) facets in the center of the right eye. Scale bars: A, 200 μm; B, 100 μm; C, 10 μm.

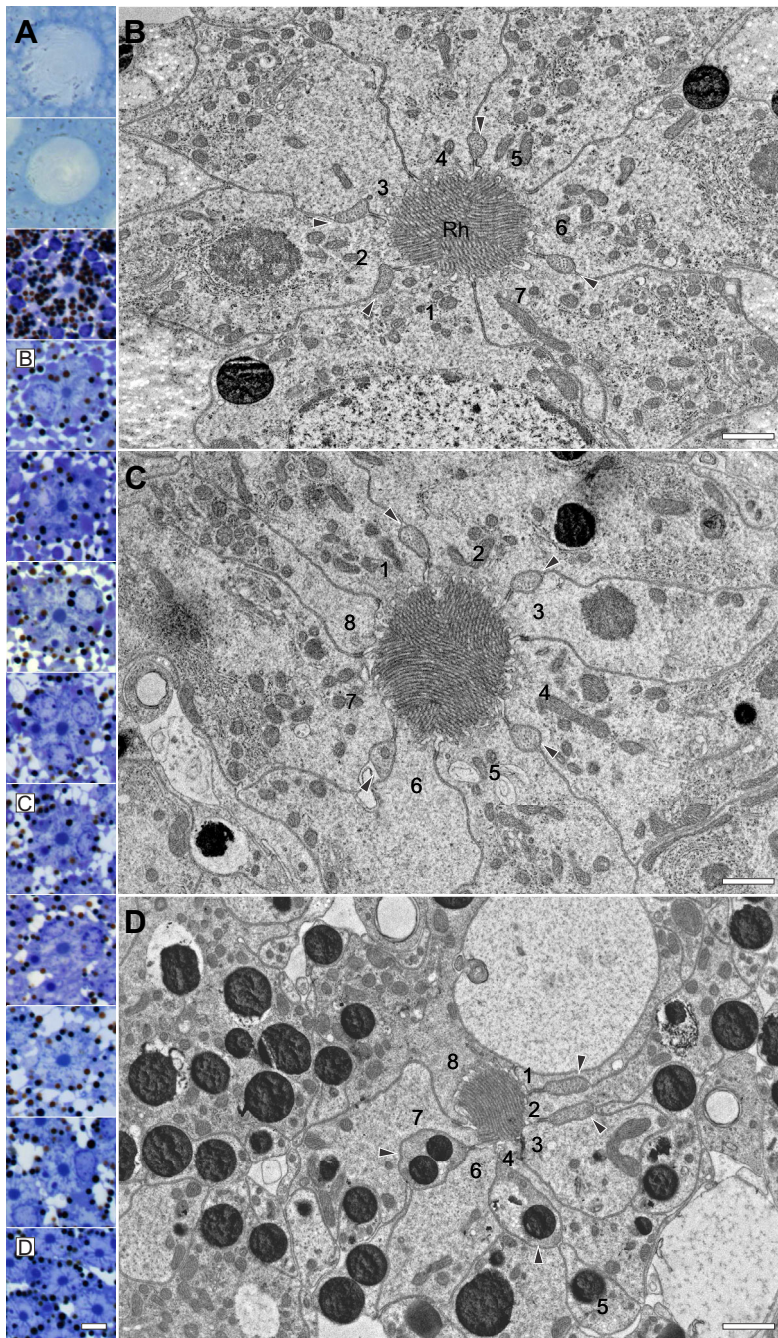


Fig. 3. Retinal cross-sections. (A) Light micrographs showing sections taken at 30 μm intervals. (B–D) Transmission electron micrographs of sections at 180, 240 and 300 μm , respectively, from the eye surface (as indicated in A). Sections are from three different ommatidia. Numbers indicate photoreceptor identity. Rh, rhabdom. Arrowheads indicate crystalline cone extensions. Scale bars: A, 5 μm ; B–D, 1 μm .

CCEs, while other photoreceptor cells are contacted by a single CCE. Cell R8 is not bordered by the CCE until the most proximal level. The CCE pattern could be used to identify the ommatidial orientations in transmission electron micrographs (Fig. 4; Fig. S2).

The ommatidia occur in two, mirror-symmetrical (chiral) forms (Fig. 4A). Both chiral forms of the ommatidia in the distal (Fig. S2) and in the proximal (Fig. 4) retina are semi-randomly oriented, i.e. the homologous photoreceptors in adjacent ommatidia assume different orientations with respect to the body axes, but preferentially along a single dorso-ventral hemisphere. In the large transmission electron micrograph in Fig. 4B containing 24 ommatidia in the central proximal retina, the proximal rhabdoms are oriented randomly around the horizontal axis; the two chiral forms of ommatidia are also distributed randomly. The chiral forms seem to form homogeneous patches, but we note that these are present in

any random ommatidial array with at least two subtypes. In three ommatidia (marked with white arrows in Fig. 4B), only the rhabdom orientation, but not chirality, could be determined. Chirality could be determined in $\sim 50\%$ of ommatidia in the best fixed light microscopic sections at high magnification and elevated contrast (Fig. 4C; the section depicts a part of the retina, different from that in Fig. 4A,B, but the same as in Fig. 4D). There, CCEs could be resolved as darker spots between photoreceptor cell somata (circular insets in Fig. 4C). The analysis of four light micrographs of different regions of the proximal retina in both sexes (original high-resolution micrographs have been deposited in figshare: <https://doi.org/10.6084/m9.figshare.12236195.v1>) revealed the random distribution of CW- and CCW-oriented ommatidia (Fig. 4D–G). The CW:CCW ratio was not significantly different among the different sections ($\chi^2=3.76$, d.f.=3, $P>0.1$) and between sexes ($\chi^2=1.50$, d.f.=1,

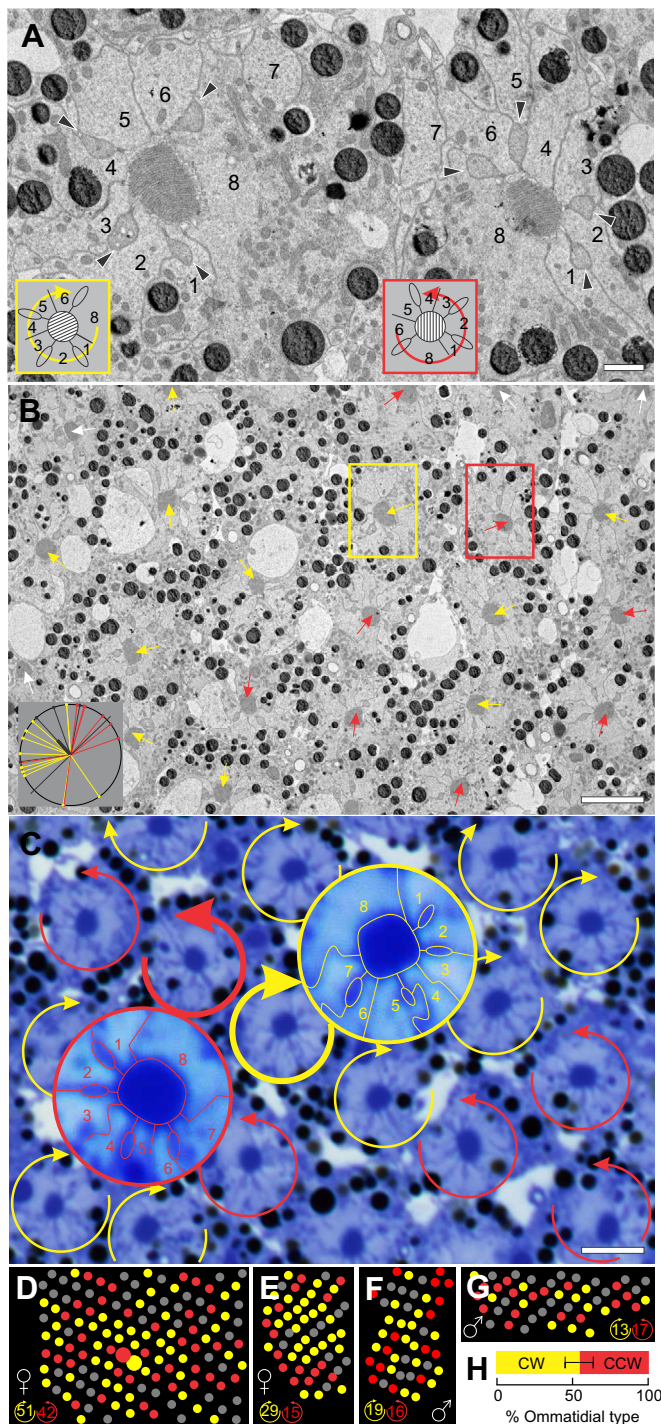


Fig. 4. Retinal mosaic. Cross-sections of the central proximal retina, where the rhabdoms consist mostly of the rhabdomere of R8. (A) Electron micrograph of two mirror-symmetric ommatidia with clockwise (CW)- and counterclockwise (CCW)-oriented photoreceptors (photoreceptor arrangements schematized in insets; yellow indicates CW orientation, red indicates CCW orientation). Numbers indicate photoreceptor cell identity as in Fig. 3; arrowheads indicate crystalline cone extensions (CCEs). The rhabdom on the left is magnified in Fig. S1. (B) Electron micrograph with 24 ommatidia; those in the yellow and red boxes are magnified in A. Arrows indicate the approximate microvillar orientation. White arrows indicate ommatidia where chirality could not be determined. Inset, superimposed microvillar orientations of the ommatidia in the slice; yellow, red and black lines indicate the orientation of microvilli (mostly of R8) in CW, CCW and undetermined ommatidia, respectively; black bar indicates the mean orientation; dotted line indicates the dorsoventral axis. (C) Light micrograph of another region of the eye in A and B with 19 mirror-symmetric, randomly arranged ommatidia. Arrows indicate the numbering order of photoreceptor cells. Bold arrows indicate ommatidia in circular insets, magnified and contrasted to visualize the membranes and CCEs that were used to determine chirality. (D, E) Maps of chiral ommatidia in four regions of the proximal retina in a female and male beetle; yellow, red and gray dots indicate CW, CCW and undetermined ommatidia; large dots in D indicate the position of magnified ommatidia in C. Sex and ommatidial counts are indicated at the bottom. (H) Fraction of CW and CCW ommatidia in D–G (mean \pm s.d.). Scale bars: A, 1 μ m; B, C, 5 μ m.

space. Most of the cells were maximally sensitive to green light with low polarization sensitivity ($\lambda_{\max}=540$ nm, polarization sensitivity PS=1.8 \pm 0.4, $N=11$; Fig. 5D). Stable recordings were obtained in two spectral classes of cells with moderate polarization sensitivity, blue-sensitive cells ($\lambda_{\max}=430$ nm, PS=3.4 \pm 0.7, $N=10$; Fig. 5C) and UV-sensitive cells ($\lambda_{\max}=350$ nm, PS=2.4 \pm 0.6, $N=12$; Fig. 5B), respectively. Some UV-sensitive cells had low polarization sensitivity and a peak shifted to shorter wavelengths ($\lambda_{\max}=335$ nm, PS=1.5, 1.6, $N=2$; Fig. 5A). A few units, termed broadband, had two spectral peaks in UV and green and low polarization sensitivity ($\lambda_{\max}=350$ nm, 540 nm, PS \approx 1–1.25, $N=2$; Fig. 5E), which in one unit was also phase-shifted between UV and green. Lastly, we found red-sensitive cells ($\lambda_{\max}=600$ nm, $N=2$; Fig. 5F); the polarization sensitivity could be determined in one cell (PS=2.5). Measurements of ERG with selective chromatic adaptation revealed the existence of three spectral classes (UV, blue and green), but failed to convincingly show the existence of the red receptors (Fig. S3). They are probably outnumbered by the major (UV, blue and green) receptor classes and thus masked in mass recordings.

DISCUSSION

Our study has revealed that flathead oak borers have compound eyes with a rich set of spectral receptors and a highly unusual, novel type of retinal mosaic, composed of randomly rotated and chiral ommatidia. The results possibly hold for all jewel beetles, because the retinal architecture of the European jewel beetle *C. undatus* is virtually identical to that of *Curis caloptera*, a jewel beetle from Australia (Gokan and Meyer-Rochow, 1984). Both species have orderly arranged crystalline cone extensions, eight receptors per ommatidium, two of them having rhabdomeres in tiers, and randomly rotated ommatidia.

Insects belonging to orders with eight receptors per ommatidium usually have two ommatidial subtypes in the main part of the eye, housing two specific combinations of spectral receptors. In flies, these are the yellow and pale ommatidial subtypes with combinations of UV+green and UV+blue central receptors, respectively, occurring in a 0.65 yellow:0.35 pale ratio (Wernet et al., 2015). It is therefore tempting to speculate that the two chiral subtypes in jewel beetles, occurring in a 0.55 CW:0.45 CCW ratio,

$P>0.1$). The average CW:CCW ratio in all analyzed sections was 0.55 \pm 0.09:0.45 \pm 0.09 (mean \pm s.d.; Fig. 4H). The varying ommatidial orientation and random distribution of the two chiral subtypes indicate that polarization sensitivity angular maxima of the photoreceptor cells are expected to be distributed randomly.

Four major spectral classes of photoreceptors

Intracellular recordings yielded 41 cells with full characterization of spectral and polarization sensitivity (Fig. 5). Spectral sensitivity was not sexually dimorphic, as all spectral classes were found in both sexes. As expected from the anatomy, the angular maxima of polarization sensitivity were distributed randomly across the angular

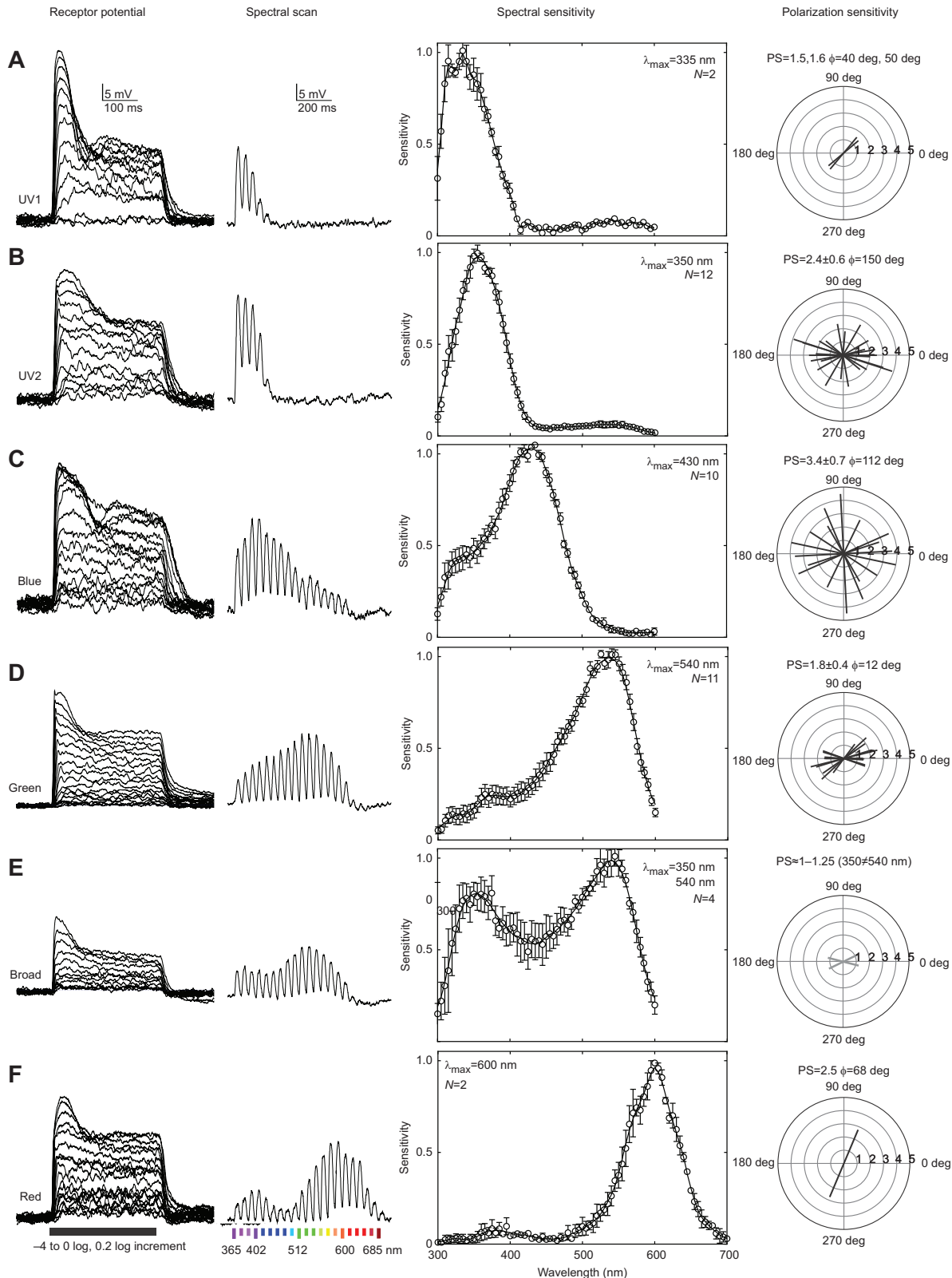


Fig. 5. Spectral and polarization sensitivity of the photoreceptors. Single-cell recordings in retinal photoreceptors, classified in rows according to spectral sensitivity. From left to right: receptor potential evoked by 300 ms light pulses at the spectral peak, intensity graded from -4 log to 0 log units in 0.2 log increments; responses to a spectral sequence of isoquantal monochromatic LED pulses; spectral sensitivity, scanned in 5 nm steps with indicated spectral peaks and cell counts (circles and bars indicate means \pm s.e.m., interpolated curve obtained by smoothing); polarization sensitivity (PS, mean \pm s.d.) and mean angular maxima (ϕ) (lines indicate individual cells). (A) UV-sensitive cells with $\lambda_{\max}=335$ nm and low PS. (B) UV-sensitive cells with $\lambda_{\max}=350$ nm and higher PS. (C) Blue-sensitive cells with $\lambda_{\max}=430$ nm. (D) Green-sensitive cells with $\lambda_{\max}=540$ nm. (E) Broadband-sensitive cells with $\lambda_{\max}=350$ and 540 nm. (F) Red-sensitive cells with $\lambda_{\max}=600$ nm.

follow the yellow:pale division and are built of two specific spectral combinations of receptors. However, we note that flies are phylogenetically advanced compared with beetles; the ancestral groups include locusts and leafhoppers (Misof et al., 2014), where the ommatidia have a combination of UV+green or blue+green receptors (Schmelting et al., 2014; Wakakuwa et al., 2014). In principle, the two structural subtypes in jewel beetles could house the combinations of UV1+blue and UV2+green receptors. Regardless, we remain skeptical about the possible link between ommatidial structure (chirality) and spectral combinations, as in other insect groups, chirality does not coincide with the division of ommatidial subtypes. In flies and honeybees, chirality corresponds only to the mirror symmetry of ommatidia across the equator (Hardie, 1985; Wehner et al., 1975), while in dragonflies, the chiral ommatidia (which were also identified with crystalline cone extensions) can be found in the left and right eye, respectively (Arnett-Kibel and Meinertzhagen, 1983).

Compound eyes of *Coraebus* harbor a full spectral set of photoreceptors, possibly enabling the beetle to use tetrachromatic color vision, based on UV, blue, green and red spectral channels. The jewel beetles nevertheless have the necessary receptors to reliably recognize complex spectral cues, such as cuticular reflections or purple traps. Consequently, carefully designed color traps could prove to be very effective in the control of this and possibly closely related (e.g. *Agrilus* spp.) pest species.

Three of the six receptor classes in *C. undatus* require further study: the broadband and the two classes of UV receptors. The broadband-sensitive cells may represent photoreceptors that express more than a single opsin (e.g. Arikawa et al., 2003), or electrically coupled UV and green receptors. Furthermore, whether the two classes of UV receptors are indeed distinct has to be checked with more recordings and opsin analysis.

Our finding of the blue and red receptor classes deserves special attention. The existence of a blue receptor class confirms the report that jewel beetles have indeed overcome the loss of the blue opsin gene, most likely via UV opsin gene duplication (Lord et al., 2016). A red receptor was found before in Coleoptera, viz. the 630 nm receptor of glaphyrid beetles, pollinators of red flowers (Martínez-Harms et al., 2012). The spectral sensitivity (half-width 79 nm of the spectrum of Fig. 5F versus 82 nm of fig. 2C of Martínez-Harms et al., 2012) is much narrower than the absorbance spectrum of a 600 nm opsin (template half-width 120 nm; Stavenga et al., 1993), possibly due to filtering by screening pigments, such as occurs in butterflies (Arikawa et al., 1999). However, perirhabdomal pigments that could represent candidate spectral filters are absent in anatomical sections. In a fused rhabdom, mutual screening of the visual pigments is inevitable, as can also be seen from the spectral sensitivity of the green receptor, which is skewed towards longer wavelengths (Fig. 5D). One cell that is expected to have strongly altered spectral sensitivity due to rhabdom filtering is R8, which occupies most of the basal rhabdom, similar to the basal R9 in butterflies (Shimohigashi and Tominaga, 1991). Whether the red receptor's narrow spectral sensitivity is caused by optical or electrical interactions remains to be demonstrated.

Photoreceptors from all spectral classes had moderate polarization sensitivity (average across all spectral classes, $PS=2.4\pm 0.7$), which, among beetles with apposition optics, is similar to that of weevils ($PS\approx 2$) (Ilić et al., 2016), but lower than in ladybugs ($PS\approx 3-5$) (Lin, 1993). The highest values ($PS>4$) were found in some cells from the 360 nm UV and the 430 nm blue receptor classes, possibly indicating that these cells had shorter rhabdomeres with less self-screening that reduces PS (Snyder, 1973) and perhaps occur in tiers,

like the fly central photoreceptors. Overall, PS of *C. undatus* is comparable to that found in, for example, butterflies (*Papilio*: $PS\approx 1.6-4.1$; *Pieris*: $PS\approx 1.1-2.9$) (Bandai et al., 1992; Blake et al., 2019b), which are known to either utilize object-directed polarization vision or suffer from polarization-based color artifacts (Kelber et al., 2001; Kinoshita et al., 2011; Blake et al., 2019a). However, to mediate polarization vision, the photoreceptors of jewel beetles should occur in orthogonal opponent pairs, located in an ordered array across the retina, similar to that in horseflies or butterflies (Blake et al., 2019b; Meglič et al., 2019). To demonstrate the existence of a suitable cellular substrate, cellular identity must be determined with dye injections; this could not be completed in our study because of the limited supply of insects. Additionally, systematic serial sections are required to show that any of these receptors form orthogonal opponent pairs. Nevertheless, the finding that the adjacent ommatidia in *C. undatus* retina are randomly rotated implies that the retinal substrate for polarization vision in jewel beetles is at least very different from that in the other insects with non-celestial polarization vision. It is likely that the signals from randomly rotated adjacent spectral receptors with phase-shifted polarization sensitivity are pooled at the level of the early interneurons (Heath et al., 2020) where the polarization-induced signals are thus cancelled out. Hence, the rotated and chiral ommatidia of jewel beetles represent a novel solution for preventing polarization-induced artifacts and somewhat resemble the twisting rhabdomeres in honeybees and flies. Alternatively, we acknowledge the possibility that the beetles have evolved interneurons that receive signals from receptors in the main retina with microvilli, oriented under specific angles. Such interneurons have been found downstream of the dorsal rim area in locusts (Labhart et al., 2001; Bech et al., 2014). They receive signals from groups of ommatidia with different (fan-shaped) microvillar orientations and act as matched filters for the detection of polarization pattern in the sky (Wehner, 1987). Obviously, behavioral experiments are needed to probe the existence of polarization vision and test the color vision of jewel beetles.

Acknowledgements

The authors are grateful to Alenka Gril for help with the statistical analysis, and to Doekele Stavenga and two anonymous reviewers for critical reading of the manuscript.

Competing interests

The authors declare no competing or financial interests.

Author contributions

Conceptualization: A.M., C.Q., G.B.; Methodology: A.M., C.Q., K.A., G.B.; Formal analysis: A.M., G.B.; Investigation: A.M., M.I., C.Q., K.A., G.B.; Resources: C.Q., G.B.; Data curation: G.B.; Writing - original draft: A.M., G.B.; Writing - review & editing: A.M., M.I., C.Q., K.A., G.B.; Supervision: G.B.; Project administration: G.B.; Funding acquisition: G.B.

Funding

This material is based upon work supported by the Air Force Office of Scientific Research under Award No. FA9550-19-1-7005, the Slovenian research agency ARRS (Javna Agencija za Raziskovalno Dejavnost RS grant P3-0333 to G.B.) and the Japan Society for the Promotion of Science (Kaken-hi 18H05273 and 18F18807 to K.A.). M.I. is a Japan Society for the Promotion of Science postdoctoral fellow. We are grateful to the Generalitat de Catalunya for financial support to C.Q.

Data availability

The original light micrographs in high resolution are available from figshare: <https://doi.org/10.6084/m9.figshare.12236195.v1>

Supplementary information

Supplementary information available online at <https://jeb.biologists.org/lookup/doi/10.1242/jeb.225920.supplemental>

References

- Arikawa, K.** (2017). The eyes and vision of butterflies. *J. Physiol.* **595**, 5457–5464. doi:10.1113/JP273917
- Arikawa, K., Scholten, D. G. W., Kinoshita, M. and Stavenga, D. G.** (1999). Tuning of photoreceptor spectral sensitivities by red and yellow pigments in the butterfly *Papilio xuthus*. *Zoolog. Sci.* **16**, 17–24. doi:10.2108/zsj.16.17
- Arikawa, K., Mizuno, S., Kinoshita, M. and Stavenga, D. G.** (2003). Coexpression of two visual pigments in a photoreceptor causes an abnormally broad spectral sensitivity in the eye of the butterfly *Papilio xuthus*. *J. Neurosci.* **23**, 4527–4532. doi:10.1523/JNEUROSCI.23-11-04527.2003
- Armett-Kibel, C. and Meinertzhagen, I. A.** (1983). Structural organization of the ommatidium in the ventral compound eye of the dragonfly *Sympetrum*. *J. Comp. Physiol.* **151**, 285–294. doi:10.1007/BF00623905
- Bandai, K., Arikawa, K. and Eguchi, E.** (1992). Localization of spectral receptors in the ommatidium of butterfly compound eye determined by polarization sensitivity. *J. Comp. Physiol. A* **171**, 289–297. doi:10.1007/BF00223959
- Bech, M., Homberg, U. and Pfeiffer, K.** (2014). Receptive fields of locust brain neurons are matched to polarization patterns of the sky. *Curr. Biol.* **24**, 2124–2129. doi:10.1016/j.cub.2014.07.045
- Belušič, G., Ilić, M., Meglič, A. and Pirih, P.** (2016). A fast multispectral light synthesiser based on LEDs and a diffraction grating. *Sci. Rep.* **6**, 32012. doi:10.1038/srep32012
- Blake, A. J., Go, M. C., Hahn, G. S., Grey, H., Couture, S. and Gries, G.** (2019a). Polarization of foliar reflectance: novel host plant cue for insect herbivores. *Proc. R. Soc. B* **286**, 20192198. doi:10.1098/rspb.2019.2198
- Blake, A. J., Pirih, P., Qiu, X., Arikawa, K. and Gries, G.** (2019b). Compound eyes of the small white butterfly *Pieris rapae* have three distinct classes of red photoreceptors. *J. Comp. Physiol. A* **205**, 553–565. doi:10.1007/s00359-019-01330-8
- Chen, P.-J., Belušič, G. and Arikawa, K.** (2020). Chromatic information processing in the first optic ganglion of the butterfly *Papilio xuthus*. *J. Comp. Physiol. A* **206**, 199–216. doi:10.1007/s00359-019-01390-w
- Domingue, M. J. and Baker, T. C.** (2012). A multidisciplinary approach for developing tools to monitor invasive buprestid beetle species. In *Invasive Species: Threats, Ecological Impact and Control Methods*, Vol. 3 (ed. J. J. Blanco and A. T. Fernandes), pp. 77–100. Nova, Hauppauge: Nova Science Publishers Inc.
- Francese, J. A., Crook, D. J., Fraser, I., Lance, D. R., Sawyer, A. J. and Mastro, V. C.** (2010). Optimization of trap color for emerald ash borer (Coleoptera: Buprestidae). *J. Econ. Entomol.* **103**, 1235–1241. doi:10.1603/EC10088
- Fürstenau, B., Quero, C., Riba, J. M., Rosell, G. and Guerrero, A.** (2015). Field trapping of the flathead oak borer *Coroebus undatus* (Coleoptera: Buprestidae) with different traps and volatile lures. *Insect Sci.* **22**, 139–149. doi:10.1111/1744-7917.12138
- Gokan, N. and Meyer-Rochow, V.** (1984). Fine-structure of the compound eye of the buprestid beetle *Curis caloptera* (Coleoptera, Buprestidae). *Z. Mikrosk. Anat. Forsch.* **98**, 17–35.
- Hardie, R. C.** (1985). Functional organization of the fly retina. In *Progress in Sensory Physiology* (ed. D. Ottoson), pp. 1–79: Springer.
- Hariyama, T., Hironaka, M., Takaku, Y., Horiguchi, H. and Stavenga, D.** (2005). The leaf beetle, the jewel beetle, and the damselfly; insects with a multilayered show case. In *Structural Colors in Biological Systems—Principles and Applications* (ed. S. Kinoshita and S. Yoshioka), pp. 153–176. Osaka: Osaka University Press.
- Heath, S. L., Christenson, M. P., Oriol, E., Saavedra-Weisenhaus, M., Kohn, J. R. and Behnia, R.** (2020). Circuit mechanisms underlying chromatic encoding in *Drosophila* photoreceptors. *Curr. Biol.* **30**, 264–275.e8. doi:10.1016/j.cub.2019.11.075
- Ilić, M., Pirih, P. and Belušič, G.** (2016). Four photoreceptor classes in the open rhabdom eye of the red palm weevil, *Rynchophorus ferrugineus* Olivier. *J. Comp. Physiol. A* **202**, 203–213. doi:10.1007/s00359-015-1065-9
- Imrei, Z., Lohonyai, Z., Muskovits, J., Matula, E., Vuts, J., Fail, J., Gould, P. J. L., Birkett, M. A., Tóth, M. and Domingue, M. J.** (2020). Developing a non-sticky trap design for monitoring jewel beetles. *J. Appl. Entomol.* **144**, 224–231. doi:10.1111/jen.12727
- Jackowska, M., Bao, R., Liu, Z., McDonald, E. C., Cook, T. A. and Friedrich, M.** (2007). Genomic and gene regulatory signatures of cryptozoic adaptation: loss of blue sensitive photoreceptors through expansion of long wavelength-opsin expression in the red flour beetle *Tribolium castaneum*. *Front. Zool.* **4**, 24. doi:10.1186/1742-9994-4-24
- Kelber, A., Thunell, C. and Arikawa, K.** (2001). Polarisation-dependent colour vision in *Papilio* butterflies. *J. Exp. Biol.* **204**, 2469–2480.
- Kinoshita, M., Yamazato, K. and Arikawa, K.** (2011). Polarization-based brightness discrimination in the foraging butterfly, *Papilio xuthus*. *Philos. Trans. R. Soc. B Biol. Sci.* **366**, 688–696. doi:10.1098/rstb.2010.0200
- Labhart, T., Petzold, J. and Helbling, H.** (2001). Spatial integration in polarization-sensitive interneurons of crickets: a survey of evidence, mechanisms, and benefits. *J. Exp. Biol.* **204**, 2423–2430.
- Labhart, T.** (2016). Can invertebrates see the e-vector of polarization as a separate modality of light? *J. Exp. Biol.* **219**, 3844–3856. doi:10.1242/jeb.139899
- Lin, J.-T.** (1993). Identification of photoreceptor locations in the compound eye of *Coccinella septempunctata* Linnaeus (Coleoptera, Coccinellidae). *J. Insect Physiol.* **39**, 555–562. doi:10.1016/0022-1910(93)90037-R
- Lord, N. P., Plimpton, R. L., Sharkey, C. R., Suvorov, A., Lelito, J. P., Willardson, B. M. and Bybee, S. M.** (2016). A cure for the blues: opsin duplication and subfunctionalization for short-wavelength sensitivity in jewel beetles (Coleoptera: Buprestidae). *BMC Evol. Biol.* **16**, 107. doi:10.1186/s12862-016-0674-4
- Martínez-Harms, J., Vorobyev, M., Schorn, J., Shmida, A., Keasar, T., Homberg, U., Schmeling, F. and Menzel, R.** (2012). Evidence of red sensitive photoreceptors in *Pygopleurus israelitus* (Glaphyridae: Coleoptera) and its implications for beetle pollination in the southeast Mediterranean. *J. Comp. Physiol. A* **198**, 451–463. doi:10.1007/s00359-012-0722-5
- Meglić, A., Ilić, M., Pirih, P., Škorjanc, A., Wehling, M. F., Kreft, M. and Belušič, G.** (2019). Horsefly object-directed polarotaxis is mediated by a stochastically distributed ommatidial subtype in the ventral retina. *Proc. Natl. Acad. Sci. USA* **116**, 21843–21853. doi:10.1073/pnas.1910807116
- Misof, B., Liu, S., Meusemann, K., Peters, R. S., Donath, A., Mayer, C., Frandsen, P. B., Ware, J., Flouri, T., Beutel, R. G. et al.** (2014). Phylogenomics resolves the timing and pattern of insect evolution. *Science* **346**, 763–767. doi:10.1126/science.1257570
- Poland, T. M., Petrice, T. R. and Ciaramitaro, T. M.** (2019). Trap designs, colors, and lures for emerald ash borer detection. *Front. For. Global Change* **2**, 80. doi:10.3389/ffgc.2019.00080
- Schenk, F., Wilts, B. D. and Stavenga, D. G.** (2013). The Japanese jewel beetle: a painter's challenge. *Bioinspir. Biomim.* **8**, 045002. doi:10.1088/1748-3182/8/4/045002
- Schmeling, F., Wakakuwa, M., Tegtmeyer, J., Kinoshita, M., Bockhorst, T., Arikawa, K. and Homberg, U.** (2014). Opsin expression, physiological characterization and identification of photoreceptor cells in the dorsal rim area and main retina of the desert locust, *Schistocerca gregaria*. *J. Exp. Biol.* **217**, 3557–3568. doi:10.1242/jeb.108514
- Sharkey, C. R., Fujimoto, M. S., Lord, N. P., Shin, S., McKenna, D. D., Suvorov, A., Martin, G. J. and Bybee, S. M.** (2017). Overcoming the loss of blue sensitivity through opsin duplication in the largest animal group, beetles. *Sci. Rep.* **7**, 8. doi:10.1038/s41598-017-00061-7
- Shimohigashi, M. and Tominaga, Y.** (1991). Identification of UV, green and red receptors, and their projection to lamina in the cabbage butterfly, *Pieris rapae*. *Cell Tissue Res.* **263**, 49–59. doi:10.1007/BF00318399
- Smola, U. and Wunderer, H.** (1981). Fly rhabdomeres twist *in vivo*. *J. Comp. Physiol.* **142**, 43–49. doi:10.1007/BF00605474
- Snyder, A. W.** (1973). Polarization sensitivity of individual retinula cells. *J. Comp. Physiol.* **83**, 331–360. doi:10.1007/BF00696351
- Stavenga, D. G., Smits, R. P. and Hoenders, B. J.** (1993). Simple exponential functions describing the absorbance bands of visual pigment spectra. *Vision Res.* **33**, 1011–1017. doi:10.1016/0042-6989(93)90237-Q
- Stavenga, D. G., Wilts, B. D., Leertouwer, H. L. and Hariyama, T.** (2011). Polarized iridescence of the multilayered elytra of the Japanese jewel beetle, *Chrysochroa fulgidissima*. *Philos. Trans. R. Soc. B Biol. Sci.* **366**, 709–723. doi:10.1098/rstb.2010.0197
- Vigneron, J. P., Rassart, M., Vandenberg, C., Lousse, V., Deparis, O., Biró, L. P., Dedouaire, D., Cornet, A. and Defrance, P.** (2006). Spectral filtering of visible light by the cuticle of metallic woodboring beetles and microfabrication of a matching bioinspired material. *Phys. Rev. E* **73**, 041905. doi:10.1103/PhysRevE.73.041905
- Wakakuwa, M., Stewart, F., Matsumoto, Y., Matsunaga, S. and Arikawa, K.** (2014). Physiological basis of phototaxis to near-infrared light in *Nephotettix cincticeps*. *J. Comp. Physiol. A* **200**, 527–536. doi:10.1007/s00359-014-0892-4
- Wehner, R.** (1987). Matched filters—neural models of the external world. *J. Comp. Physiol. A* **161**, 511–531. doi:10.1007/BF00603659
- Wehner, R. and Bernard, G. D.** (1993). Photoreceptor twist: a solution to the false-color problem. *Proc. Natl. Acad. Sci. USA* **90**, 4132–4135. doi:10.1073/pnas.90.9.4132
- Wehner, R., Bernard, G. D. and Geiger, E.** (1975). Twisted and non-twisted rhabdoms and their significance for polarization detection in the bee. *J. Comp. Physiol.* **104**, 225–245. doi:10.1007/BF01379050
- Wernet, M. F., Perry, M. W. and Desplan, C.** (2015). The evolutionary diversity of insect retinal mosaics: common design principles and emerging molecular logic. *Trends Genet.* **31**, 316–328. doi:10.1016/j.tig.2015.04.006

Supplementary information

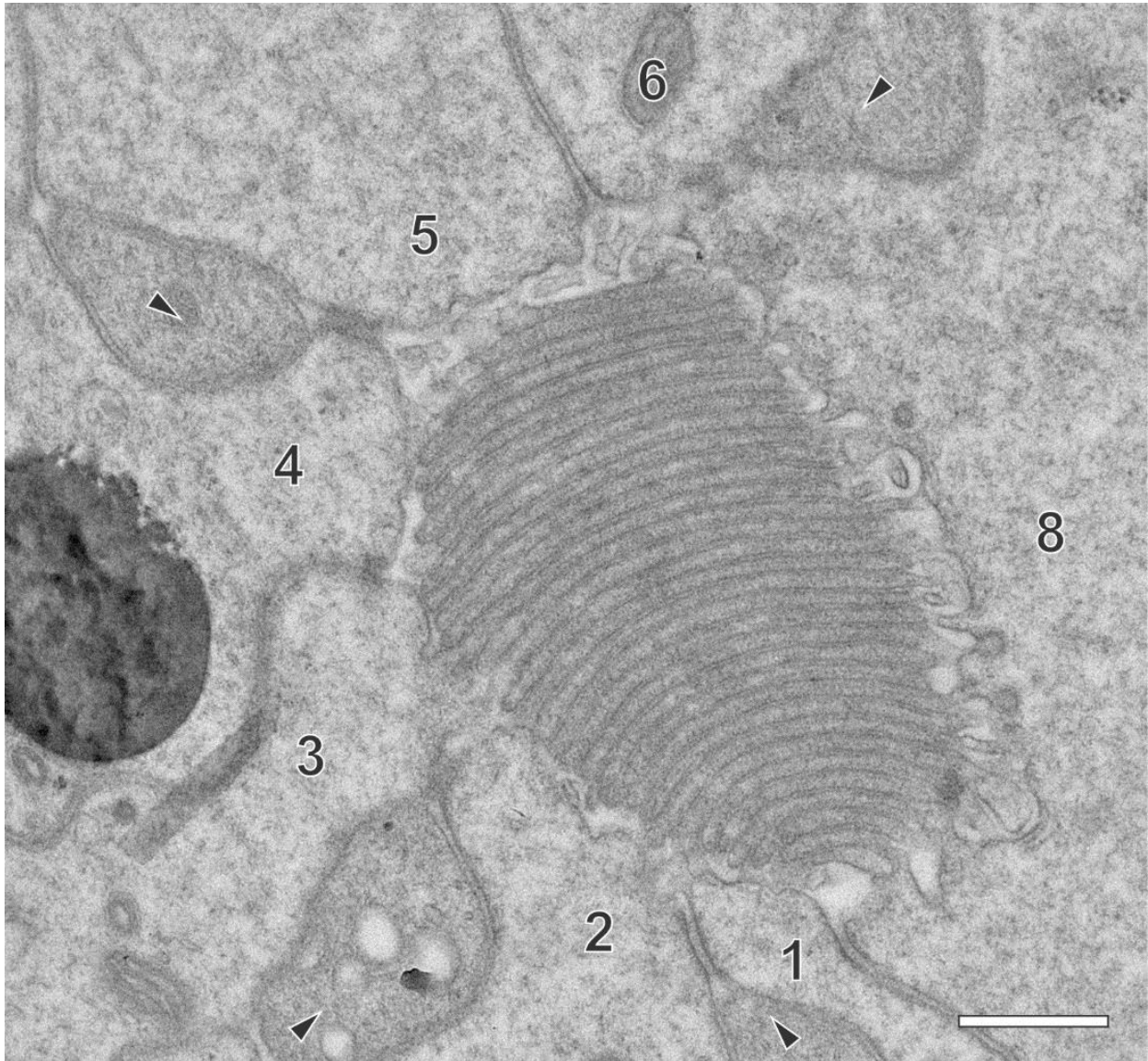


Fig. S1 Proximal rhabdom.

Electron micrograph of the ommatidium on the left in Fig. 4A. Most microvilli are contributed by R8, some by R3 and R2. Numbers indicate photoreceptor cell identity, arrowheads indicate crystalline cone extensions. Scale bar, 500 nm.

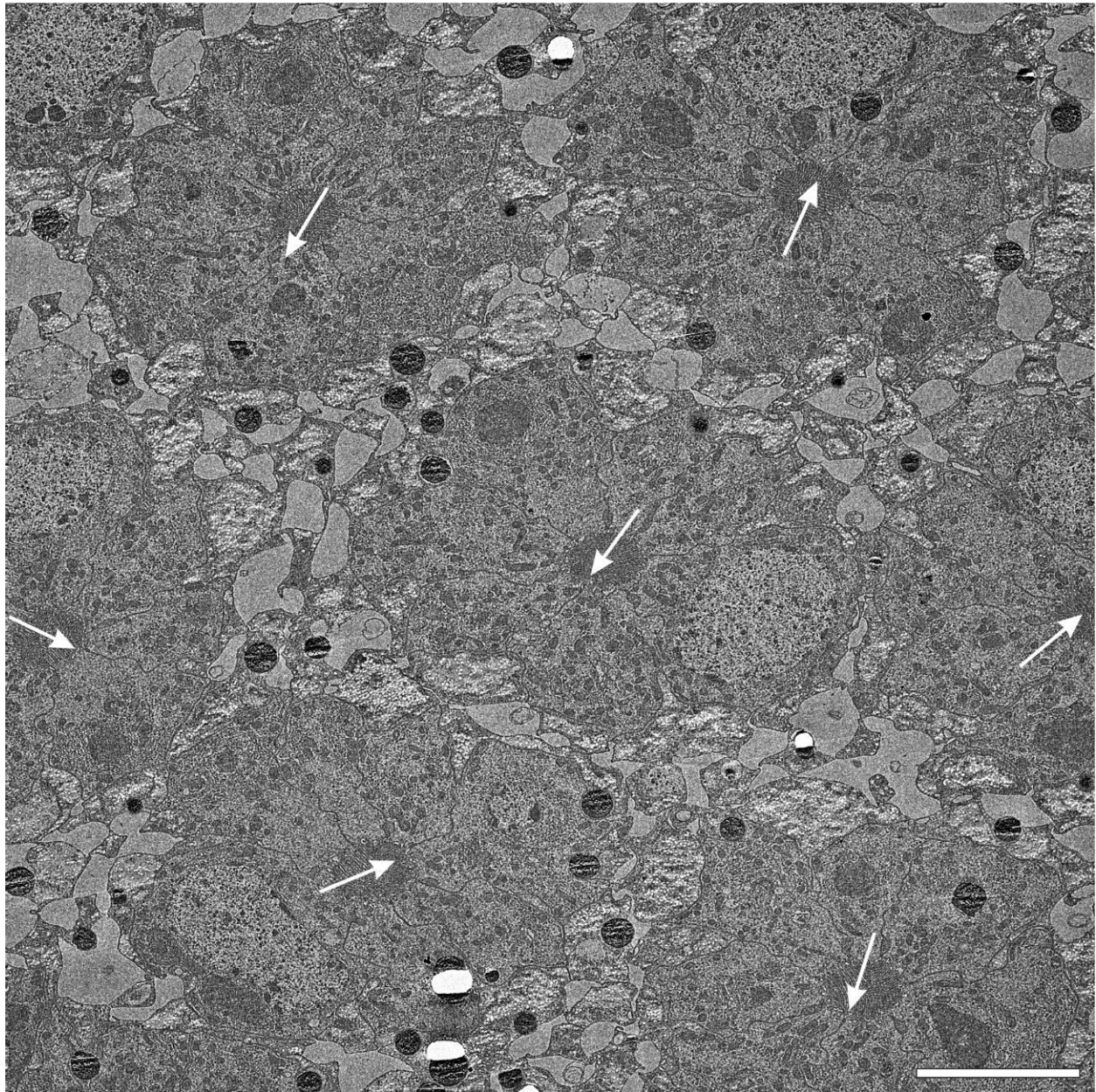


Fig. S2 Cross section of the central distal retina.

7 ommatidia with randomly oriented rhabdoms. Arrows indicate the direction R2 – R5/6. Scale bar 5 μ m.

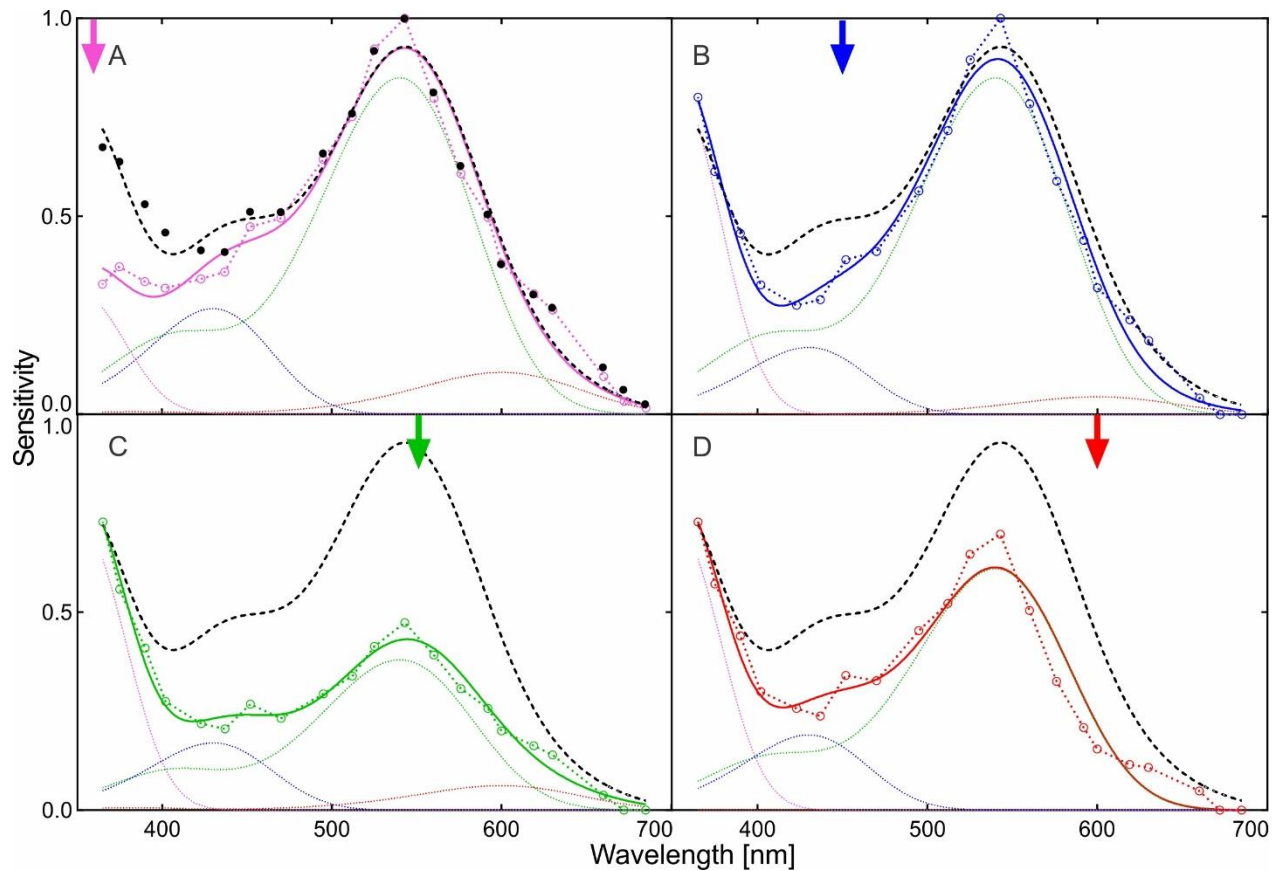


Fig. S3 Spectral sensitivity of a compound eye, determined with electroretinography (ERG). Dashed black curve, linear sum of rhodopsin templates (small dotted curves, λ_{\max} =350, 430, 540, 600 nm) fitted to the sensitivity of dark-adapted eye (full black circles in A). Solid curves, linear sums of templates, fitted to sensitivities of eyes (empty colored circles and dotted lines), adapted to UV (A, 360 nm), blue (B, 440 nm), green (C 540 nm) and red (D, 600 nm) light (all adapting lights, $\sim 10^{11}$ quanta $\text{cm}^{-2} \text{s}^{-1}$).